Dalton Transactions

Accepted Manuscript

This is an *Accepted Manuscript*, which has been through the RSC Publishing peer review process and has been accepted for publication.

Accepted Manuscripts are published online shortly after acceptance, which is prior to technical editing, formatting and proof reading. This free service from RSC Publishing allows authors to make their results available to the community, in citable form, before publication of the edited article. This *Accepted Manuscript* will be replaced by the edited and formatted *Advance Article* as soon as this is available.

To cite this manuscript please use its permanent Digital Object Identifier (DOI®), which is identical for all formats of publication.

More information about *Accepted Manuscripts* can be found in the **Information for Authors**.

Please note that technical editing may introduce minor changes to the text and/or graphics contained in the manuscript submitted by the author(s) which may alter content, and that the standard **Terms & Conditions** and the **ethical guidelines** that apply to the journal are still applicable. In no event shall the RSC be held responsible for any errors or omissions in these *Accepted Manuscript* manuscripts or any consequences arising from the use of any information contained in them.

Influence of Gd^{3+} co-doping on Structural Property of $CaMoO_4$:Eu

B. P. Singh,[a] A. K. Parchur,[b*] R. S. Ningthoujam,[c] A. A. Ansari,[d] P. Singh[a] and S. B. Rai[b]

[a]*Department of Physics, Indian Institute of Technology (BHU), Varanasi, India-221005*
[b]*Department of Physics, Banaras Hindu University, Varanas, Indai-221005*
[c]*Chemistry Division Bhabha Atomic Research Centre, Mumbai, India-400085*
[d]*King Abdullah Institute for Nanotechnology, King Saud University, Riyadh, Saudi Arabia-11451*

Abstract:

A facile auto-combustion route is used for synthesis of 2 at.% Eu^{3+}-doped and Gd^{3+} (2, 5, 7 and 10 at.%) co-doped $CaMoO_4$:Eu nanoparticles. X-ray diffraction study suggests that as-prepared samples have extra impurity phases in addition to main tetragonal phase of $CaMoO_4$; and such extra phases decrease as annealing temperature increases from 600 to 900 ^oC. The crystal structure has been analysed using Rietveld program. It has space group $I4_1/a$ (88) and Z = 4 (number of $CaMoO_4$ formula units per unit cell). Average crystallite sizes of as-prepared, 600 and 900 ^oC annealed samples for 2 at.% Gd^{3+} are found to be ~33, 48 and 61 nm, respectively. The lattice strains of 5 at.% Gd^{3+} co-doped $CaMoO_4$:Eu for as-prepared and 900 ^oC are 0.001 and 0.002, respectively. Fourier transform infrared spectroscopy gives the absorption bands at ~815 and 427 cm^{-1}, which are related to asymmetric stretching and bending vibrations of MoO_4^{2-} tetrahedron. Particle morphology is studied using scanning and transmission electron microscopy (SEM and TEM); and aggregate of particles is found. X-ray photoelectron spectroscopy (XPS) is utilized to examine the oxidation states of metal ions/oxygen and oxygen ion vacancies in Gd^{3+}co-doped $CaMoO_4$:Eu. With increase of Gd^{3+} concentration, peak corresponding to Gd^{3+} ($2p_{3/2}$ and $2p_{5/2}$) binding energy could be detected.

*Corresponding author: *kareemskpa@hotmail.com*

1. Introduction

Recently, alkaline-earth metal tungstates and molybdates (scheelite type, ABO_4, A = Ca^{2+}, Sr^{2+}, Mg^{2+} and Ba^{2+}; B = Mo and W) based derivatives are important host material for rare-earth-doped phosphors because of their excellent optical and physical properties such as excellent strength, chemical, thermal stabilities, high decomposition temperature and multi-color range from blue to green-yellow-red.[1-5] Among the alkaline-earth metal molybdates, $CaMoO_4$ (having space group $I4_{1/a}$ having point group symmetry C^6_{4h} with tetragonal structure) has been used in solid-state laser, scintillators in medical devices, solar cell and fiber-optical communication.[1-7] In $CaMoO_4$, Mo^{6+} is coordinated by four oxygen atoms in tetrahedral symmetry to form MoO_4 and Ca has been coordinated by 8 oxygen atoms to form CaO_8.[5-8] [MoO_4^{2-}] tetrahedron unit efficiently absorbs light with higher absorption cross section near UV region and its photoluminescence shows broad visible range. The photoluminescence of $CaMoO_4$ doped with different lanthanide ions has been studied in order to get different colours.[1-7]

Recently, nanomaterials have been synthesized in the form of nanorods, sheets, wires, nanopores and core-shell.[9-12] Lanthanide (Ln^{3+}) doped inorganic nanomaterials are used in luminescence applications because of its resistant to photo-bleaching, superior photochemical stability, sharp emission bands, persistent photoluminescence lifetime, high chemical stability and having low toxicity.[13] Moreover, Ln^{3+} ion such as Gd^{3+} has large number of unpaired electrons in 4f orbitals which can change the relaxation time of surrounding water protons when Ln^{3+} doped nanomaterials are dispersed in water. Thus, these are also used as MRI (magnetic resonance imaging) contrast agent in medical diagnostics.[14,15] There are reports on enhancement of luminescence by core-shell, co-doping and energy transfer process.[16-19] Therefore, systematic research on the synthesis protocol, structure and its resultant effects on phosphor characteristics is necessary and worthy of pursuit. Moreover, influence of Gd^{3+}

incorporation on structural and luminescence properties of $CaMoO_4$:Eu has not been explored in literature in much detail. Many synthesis processes have been reported by different groups to synthesize $CaMoO_4$ with or without Ln^{3+} ions via Czochralski, conventional solid state reaction method, sol-gel, hydrothermal, co-precipitation and polyol methods.[5,20] Auto-combustion methods has been proven to be very much effective as one have wide range of flexibility of selection of fuels, rapid cooling process which hinders the nucleation growth of the crystallites, enabling non-agglomerated nanocrystals of high purity with nano-size regime. This methodology makes it possible to prepare nonmaterial with versatile compositions of different concentrations which is easily doped with various ions.[21]

In this work, we have prepared Gd^{3+} (0, 2, 5, 7 and 10 at.%) co-doped $CaMoO_4$:Eu nanoparticles via efficient combustion technique. Here, the urea-nitrate combustion synthesis is used. For the optimal Eu^{3+} concentration (2 at.% in our case), effect of Gd^{3+} co-doping on structure, chemical binding energies and morphology of $CaMoO_4$:Eu has been investigated in detail for as-prepared, 600 and 900 ^oC annealed samples.

2. Experimental

2.1. Sample Preparation

Combustion synthesis route was employed in order to synthesize the nanophosphors at lower temperature with high chemical homogeneity. $CaCO_3$ (99.99%, Sigma Aldrich), Eu_2O_3 (99.99%, Alfa Aesar) and Gd_2O_3 (99.99%, Alfa Aesar) and $(NH_4)_6Mo_7O_{24}.4H_2O$ (99%, Alfa Aesar) were used as a starting materials. In a typical synthesis process (e. g. 2 at.% Gd^{3+}, 2 at.% Eu^{3+} doped $CaMoO_4$)**,** 0.343 g of $CaCO_3$, 0.631 g of $(NH_4)_6Mo_7O_{24}.4H_2O$, 0.126 g of Eu_2O_3 and 0.129 g of Gd_2O_3 were dissolved together in 2 ml of 1 M nitric acid (HNO_3). The mixture was heated at 80 ^oC for the removal of excess of acid and this process was repeated at least five times with addition of 5 ml doubled distilled water. Transparent solution is obtained after 1 hour. $(NH_4)_6Mo_7O_{24}.4H_2O$ was dissolved in 20 ml of deionised

water. To this 2 g of urea was added for adjusting the pH of the solution between 8 and 9 and placed under sonication for 30 min. This was added to above solution drop wise and stirred for 2-3 h. A whitish gel like precipitate was obtained. This was placed in furnace at ~250 ^{o}C for 30 min to take place auto combustion. Powder sample so obtained was treated as as-prepared sample (ASP). ASP samples are divided into three parts. One part of the sample was annealed at 600 ^{o}C while other part at 900 ^{o}C for 4 h in ambient atmosphere at the rate of 2 ^{o}C min^{-1} in programmable electrical furnace and remaining third part was kept as such.

2.2 Characterization techniques

Structural confirmation of the phosphor was identified by X-ray diffraction (XRD) using a Rigaku miniflex-II diffractometer equipped with Ni filter using CuK_{α} radiation (1.5405 Å) at ~30 kV and ~15 mA in the range $10 \leq 2\theta/^{o} \leq 70^{o}$ with a step size of $\Delta 2\theta = 0.02^{o}$. The Fourier transform infrared (FTIR) spectrum of the sample was recorded on a Perkin - Elmer 580 B IR spectrometer using the KBr pellet technique in the range 4000-400 cm^{-1}. Sample was mixed with KBr (Sigma Aldrich, 99.99%) in 1:5 wt.% ratio and transparent pellet was prepared. The chemical binding energies of the respective ions in the sample were measured using X- ray photoelectron spectroscopy (XPS) SPECS, Germany (Mg K_{α} X-ray source, $h\nu$ = 1253.6 eV). Differential thermal (DT) and thermo-gravimetric (TG) analyses of the sample were carried out with a *Material Analysis and Characterization TG-DTA 2000* with a heating rate of 5 ^{o}C/min. Morphology of synthesized powder samples was further examined by a field emission scanning electron microscope (FESEM, JSM-6700, model JEOL, Japan). Coating of osmium had been sprayed on the sample surfaces using a Hitachi (Japan) fine coat ion sputter E-1010 unit to avoid the expected charging of the specimens before FESEM observation was performed on each time. Field emission transmission electron microscope (FE-TEM) equipped with energy disperse X-ray spectroscopy, EDX (FETEM, JEM-2100F, JEOL, Japan) operating at an accelerating voltage of 200 kV were

employed for the inspection of morphology of the samples. EDX analysis was used to confirm the presence of the constituent elements in the sample. For the TEM measurement, a small amount of Gd^{3+} co-doped $CaMoO_4$:Eu was dispersed in the methanol and placed under sonication for 30 min. A few drops of suspended monodispersed colloidal solution were put over a carbon coated copper grids. Measurements were performed on these grids after drying the samples naturally.

3. Results and Discussion

3.1. Structural Analysis

3.1.1 XRD study

XRD patterns of ASP Gd^{3+} (0, 2, 5 7 and 10 at.%) co-doped sample of $CaMoO_4$:Eu is shown in the Fig.1(a). It is evident from the figure that even as-prepared (ASP) sample shows highly crystalline behaviour with tetragonal structure. All diffraction peaks match well with JCPDS card no. 29:0351 (a = 5.226 Å, c = 11.43Å and V = 312.17Å^3). In the case of Gd^{3+}(2, 5, 7 and 10 at.%) co-doped ASP samples, some extra XRD peaks (marked with #) are observed at an angle 2θ = ~17, 19.47, 25.98, 27.39, 35.48 and 42.7˚. Such peaks are not matching with JCPDS card no. 29-0351. The intensity of these extra peak intensities increase as doping concentration of Gd^{3+} increases. Also some extra peaks are found at ~23.3, 25.6 and 26.9˚ for 10 at.% Gd^{3+} co-doped samples of $CaMoO_4$:Eu annealed at 600 ^oC. These extra peaks may be due to the $MoO_n.mH_2O$ (where m and n are numbers), carbonate, water complexes, Gd-Eu-O related compounds, or Eu^{3+} oxides present in the sample. These phases are not identified in this study. Similar types of observations have been reported for Tb^{3+} doped $CaMoO_4$.[5] However, in case of 900 ^oC annealed samples, no other traces of impurity phases have been observed. However, the intensities of diffraction peaks slightly decrease at higher Gd^{3+} co-doping concentrations. Lattice parameters of typical 5 at.% Gd^{3+}co-doped $CaMoO_4$:Eu for ASP are a = 5.239Å, c = 11.392Å, V = 313.07Å^3 and for 900 ^oC annealed

samples are a = 5.226Å, c = 11.437Å and V = 312.37Å^3. Unit cell volume calculated for ASP samples is slightly high because of the broadness of the peaks as compared to the standard JCPDS card no. 29:0351. Samples annealed at ~600 and 900 ^{o}C show slightly higher crystalline behaviour than ASP one, which are shown in Fig. 1(b) and (c), respectively. The average crystallite size of the samples was calculated by using Scherrer formula,

$$D = \frac{k\lambda}{\beta_{hkl} Cos(\theta)} \qquad (1)$$

where D *is* average crystallite size, k = 0.89, λ, wavelength and θ, Bragg's diffraction angle of the planes and β_{hkl} is the corrected full width at half maximum (*FWHM*). For β_{hkl} correction, β_{inst} (*FWHM* due to instrument) is removed using *Si* standard. Average crystallite size determined using the Scherrer formula for the 2 at.% Gd^{3+}co-doped $CaMoO_4$:Eu of ASP, 600 and 900 ^{o}C annealed samples are found to be ~33, 48 and 61 nm, respectively. Average crystallite size of the samples annealed at ~600 and 900 ^{o}C is found to increase with the Gd^{3+} doping concentration. Structure refinement of Gd^{3+} (0, 2, 5 7 and 10 at.%) co-doped $CaMoO_4$:Eu samples annealed at ~600 and 900 ^{o}C was carried out using *FullProf* software.[22] The peak profiles was modelled using Pseudo-Voigt function while background was described in terms of a six coefficient polynomial. R_{wp} (weighted-pattern factor) and S (goodness-of-fit) parameters were used as numerical criteria of the quality of fit to experimental diffraction data. Rietveld refinement patterns of Gd^{3+} (0, 2, and 10 at.%) co-doped $CaMoO_4$:Eu, for 900 ^{o}C are shown in Fig. 2(a-c). The Wyckoff positions of atoms based on space group $I4_{1/a}$ (88) and Z = 4 (number of $CaMoO_4$ formula units per unit cell) in $CaMoO_4$ unit cell are: [8]

Ca: (4b: 0, ¼, 5/8)

Mo: (4a: 0, 1/4/ 1/8)

O: (16f: x, y, z)

The Bragg reflections, difference in observed and calculated intensity are shown in figure itself. Refinement patterns of 5 and 7 at.% Gd^{3+} co-doped $CaMoO_4$:Eu, for 900 ^oC are given in electronic supplementary information Fig. S1(a), (b)(ESI†). Moreover, refinement patterns of Gd^{3+} (0, 2, 5, 7 and 10 at.%) co-doped samples of $CaMoO_4$:Eu annealed at 600 ^oC are shown in Fig. S2(a)-(e) (ESI†). The crystal structure and symmetry resembled to that of its simplified 3D polyhedral representation are shown in Fig. 2(d), which demonstrates the presence of high inversion symmetry in the lattice. As $CaMoO_4$ belong to the derivative of ABO_4 (A = Ca, Ba, Sr, Pb and B = Mo, W) with tetragonal scheelite structure having body centred inversion symmetry. A and B sites show S_4 point symmetry while its crystal structure comprises of two building block units namely, Eu/Gd/CaO_8 polyhedra and MoO_4 tetrahedra, respectively. In c direction, Eu/Gd/CaO_8 polyhedron shares four of its edges with four other Eu/Gd/CaO_8 polyhedrons through oxygen atoms. Oxygen atoms are sharing co-ordination among Eu/Gd/CaO_8 polyhedron and MoO_4 tetrahedron, respectively. Observed lattice parameters after Rietveld refinement, cell volume and average crystallite size for 600 and 900 ^oC samples for Gd^{3+} (0, 2, 5, 7 and 10 at.%) co-doped $CaMoO_4$:Eu samples are listed in Table 1. It is found that the cell volume slightly increases after Gd^{3+} incorporation in $CaMoO_4$:Eu for 900 ^oC annealed samples in comparison to samples annealed at 600 ^oC. This is may be due to ionic radii mismatch of Ca^{2+} ion as compared to Gd^{3+}/Eu^{3+}. Ionic radii of Eu^{3+} (1.06Å) and Gd^{3+} (1.05Å) are similar to Ca^{2+} (1.12Å) based on 8 coordination number (CN) [CaO_8] and Mo^{6+} has ionic radius of 0.42 Å in [MoO_4]. Therefore, Eu^{3+} and Gd^{3+} are supposed to occupy Ca^{2+} sites in spite of charge imbalance.[8,23] The micro-strain has been calculated for Gd^{3+} co-doped $CaMoO_4$ for ASP, 600 and 900 ^oC annealed samples using Williamson- Hall[24] formula which has given as:

$$\frac{\beta_{hkl}cos\theta}{\lambda} = \frac{1}{D_{hkl}} + (\epsilon_{hkl})\frac{sin\theta}{\lambda} \quad (2)$$

where β_{hkl} is the full width at half maximum (*FWHM*) of X-ray patterns, θ, the Bragg's diffraction angles, λ, the wavelength of X-ray, D_{hkl}, the effective crystallite size and ϵ_{hkl} is the micro-strain. The instrumental broadening (ϵ_{ins}) is removed by using Si standard. Micro-strain is calculated for 0, 5 and 10 at.% Gd^{3+} doped $CaMoO_4$ and the values are found to be ~0.0014, 0.0017, 0.0027 for ASP while ~0.0016, 0.0023 and ~0.0029 for 900 ^oC annealed samples, respectively. It has been inferred from the strain data that it increases with increase in Gd^{3+}concentration. Positive slope value (ϵ_{hkl}) indicates the presence of tensile strain acting on the system.[12] *Dutta et al.* have reported recently the variation in strain (0.001-0.003) in Dy^{3+} doped $CaMoO_4$. It is found that strain increases with Dy^{3+} concentration, and being relaxed by co-doping of K^+ ions in $CaMoO_4$.[25]

It is observed that pattern intensity of Gd^{3+} co-doped $CaMoO_4$:Eu is slightly less than $CaMoO_4$:Eu samples, which is due to defects created on Gd^{3+} co-doped $CaMoO_4$:Eu. Extra phases demonstrate the solubility limit of $Gd^{3+}$and Eu^{3+} ions in host lattice. It expected that up to 2 at.% of Eu^{3+} and up to 10 at.% Gd^{3+} charge compensation occurs for Ca^{2+} and oxygen ion vacancies. In the present study, nanophosphor is synthesized without any charge compensation of ions. The crystal structure are still consistent with scheelite phase with Gd^{3+} content up to 10 at.% for 600 and 900 ^oC annealed samples. Charge loss may be compensated as Ca^{2+} vacancies (V_{Ca}''). The defect equation mechanism for the Ca^{2+} vacancies can be proposed as:

$$3Ca^{2+} \rightarrow 2Eu_{Ca}^{\bullet} + V_{Ca}''$$

and

$$3Ca^{2+} \rightarrow 2Gd_{Ca}^{\bullet} + V_{Ca}''$$

In other words two Eu^{3+} or two Gd^{3+} ions must replace three Ca^{2+} sites to maintain charge balance and hence one V_{Ca}'' is created. Ionic radii mismatch among the Ca^{2+}, Eu^{3+} and Gd^{3+} are supposed to be responsible for the vacancy generation of V_{Ca}'' and creation of other point

defects in the lattice. Similar behaviour have been reported for Bi^{3+} co-doped $CaMoO_4$:5Eu^{3+}.[26]

3.1.2 FTIR study

FTIR spectra of the ASP, 600 and 900 ^oC annealed samples of 5 at.% Gd^{3+} co-doped $CaMoO_4$:Eu in the range 4000 - 400 cm^{-1} are shown in the Fig. 3. Infrared absorption spectra show the all expected vibrational modes of calcium molybdate, which confirms the phase purity of the materials. Group theory calculations show that there are having 26 modes of vibrations (Raman and infrared) for scheelite type structure which can be represented as:[27]

$$\Gamma_{(\text{Raman + Infrared})} = 3A_g + 5A_u + 5B_g + 3B_u + 5E_g + 5E_u \qquad (3)$$

where A_g, B_g and E_g are Raman-active modes. There are 13 Raman active modes observed for the $CaMoO_4$ which is represented by equation as:[28]

$$\Gamma_{(\text{Raman})} = 3A_g + 5B_g + 5E_g \qquad (4)$$

and eight infra-red active modes which is given as: [29]

$$\Gamma_{(\text{infrared})} = 4A_u + 4E_u \qquad (5)$$

Infrared bands at ~1652 and 3419 cm^{-1} correspond to bending and stretching vibrational modes of absorbed water molecules on the surface of nanoparticles.[30] Observed absorption patterns intensity decreases as annealing temperature increases. Absorption peaks appearing at ~815 cm^{-1} is occurring due to the asymmetric stretching vibration of O-Mo-O vibration in MoO_4^{2-} tetrahedron, while peak at ~427 cm^{-1} occurs due to bending vibration of Mo-O of A_u mode.[31,32] It observed that both O-Mo-O and Mo-O vibrations are slightly shifted towards lower wave number (~3-5 cm^{-1}) due to annealing the samples at 600 and 900 ^oC, which infer the lattice expansion of $CaMoO_4$ host. The red shifts in A_u mode of vibrations are responsible for lattice expansion in host. Band arises at ~1383 cm^{-1} demonstrates the presence of N-O modes of vibration of HNO_3 used in the sample preparation. Similar observation was reported in Tb^{3+} doped $CaMoO_4$.[5]

3.1.3 XPS study

The oxidation states of the constituent elements present in sample can be identified using XPS. XPS spectra of Ca, Mo and O core binding energy (BE) in ASP and 900 ^{o}C annealed samples of 0, 5 and 10 at.% Gd^{3+}co-doped $CaMoO_4$:Eu are shown in Figs. 4 and 5. Whole spectrum comprising of core BE levels of Ca, Mo, O, Eu/Gd is shown in Fig. S3(a) (ESI†) obtained in the range of 0-1000 eV. Figure 4(a) (i)-(iii) shows the XPS spectrum of Ca (2*p*) for 0, 5 and 10 at.% Gd^{3+} co-doped $CaMoO_4$:Eu ASP samples. For Gd^{3+} free $CaMoO_4$:Eu sample, the peaks are corresponding to Ca (2*p*) having core BE ~346.84 ($2p_{3/2}$) and 350.39 eV ($2p_{1/2}$) and full width at half maximum (FWHM) ~1.7 and 2.0 eV. On increasing Gd^{3+} (5 and 10 at.%) co-doping concentration, there is slight changes in BE values to higher eV. Moreover, integrated intensity ratio of ($2p_{3/2}$) to ($2p_{1/2}$) (I_{Ca}) is found to be 1.76, 1.9 and 1.47 eV for 0, 5 and 10 at.% Gd^{3+} co-doping, respectively. On annealing the sample at 900 ^{o}C, there is slight decrease in BE of Ca($2p_{3/2}$) and Ca($2p_{1/2}$) by 0.25-0.47 eV for 0, 5 and 10 at.% Gd^{3+} co-doped $CaMoO_4$:Eu samples which is shown in Fig. 4(b) (i)-(iii); and FWHM and I_{Ca} does not change significantly within the limits of error bar. These results confirm 2+ oxidation state of Ca. Fig. 4(c) (i) shows the peaks at ~232.64 and 235.77 eV, which correspond to the core BE of Mo($3d_{5/2}$) and Mo($3d_{3/2}$), respectively for ASP Gd^{3+} free $CaMoO_4$:Eu sample. Integrated intensity ratio of ($3d_{5/2}$) to ($3d_{3/2}$) (I_{Mo}) are found to be 1.36, 1.49 and 1.39 eV for 0, 5 and 10 at.% Gd^{3+} co-doping samples, respectively (Fig. 4(c) (i)-(iii)). There is no significant change in BE on Gd^{3+} co-doping. On annealing the samples at 900 ^{o}C, BE are slightly shifted to lower eV by 0.17 to 0.47 eV (Fig. 4(d) (i)-(iii)). Also, (I_{Mo}) found to be 1.39, 1.43 and 1.39 eV for 0, 5 and 10 at.% Gd^{3+} co-doping samples, respectively. The lack of any significant change in the $3d_{3/2}$-$3d_{5/2}$ BE in the Mo spectral region suggests that Mo ions remain in its Mo^{6+} state. Similar behaviour was supported in literatures[33,34] for Ca-Bi-Mo oxide and for the molybdenum phosphate glass. Notably the

peaks for Gd^{3+} and Eu^{3+} fall on ~141-148 eV. So it is bit difficult to distinguish $Eu^{3+}(4d_{3/2})$ and $Gd^{3+}(4d)$. Peak at ~141.1 eV, which corresponds to $Eu^{3+}(4d_{3/2})$ and there having no peak at ~127.1 eV corresponding to $Eu^{2+}(4d_{5/2})$ is observed. This is confirmed that the high probability of Eu^{3+} is present in the sample. It is also confirmed from excitation/emission study (not shown). Moreover, small peaks at 141.4 and 146.2 eV correspond to $Gd(2p_{3/2})$ and $Gd(2p_{5/2})$, respectively.[35] Typical XPS spectra showing core binding energy and intensity of Eu and Gd in 10 at.% ASP Gd^{3+} co-doped $CaMoO_4$:Eu is shown in Fig. S4 (ESI†). Intensity of these peaks is very small for ASP and 900 ^oC annealed samples and improves with increase of Gd^{3+} concentration. It is may be due to presence of less no of Gd^{3+}/Eu^{3+} ions presents in the sample. In addition, O(1s) spectral regions have been used to obtain the information regarding the presence of oxygen vacancies present in the sample (Fig. 5). Peaks were deconvoluted using Gaussian function. In case of ASP Gd^{3+} free $CaMoO_4$:Eu sample, two peaks are well fitted at BE ~ 529.5 (P_1) and 531.6 eV (P_2) having FWHM ~1.8 and 1.82 eV, respectively. On increasing Gd^{3+} co-doping peak position slightly changes by ± 0.1-0.4 eV (Fig. 5(a)). Similar spectra are observed upon annealing the sample at 900 ^oC (Fig. 5(b)). BE of the peaks is shifted to ~± 0.26-0.76 eV with respect to corresponding ASP samples. Overall peaks show asymmetric nature in higher BE side. Further relative area of P_2/P_1 of ASP and 900 ^oC annealed samples for 0, 5 and 10 at.% Gd^{3+}co-doped $CaMoO_4$:Eu provides an interesting features shown in Fig. S3(b) (ESI†). This is may be due to the defects and of oxygen vacancies creation on behalf of non-isovalant dopant. There are few reports which indicate that high energy side of O(1s) peak arises due to hydroxyl groups –OH or other radicals on the sample surface as CO or CO_2.[36] However, the asymmetric behaviour at high energy peak (~530.5 eV) in an O1s spectrum is signature of the presence of oxygen ion vacancy in the lattice.[37] It can be suggested that oxygen vacancy decreases with annealing sample at high temperature.

3.1.4 DT-TGA study

Thermal decomposition of ASP $CaMoO_4$:Eu in air has been studied by thermo gravimetric (TGA) and differential thermal analyses (DTA), shown in Fig. 6. TG curve shows two distinct stages of weight loss. First weight loss (~2%) step is observed between 55-140 ^oC, which is attributed to the removal of residual water molecules absorbed on the sample surface. The second weight loss (8%) is in the temperature range 140-600 ^oC accompanied by an exothermic peak at 305 ^oC in DTA curve which may be due to the further combustion of organic matrices like hydrocarbons, carbonates and nitrates. Moreover, weight loss after ~600 ^oC becomes constant and thereafter no significant loss has been observed upto 900 ^oC. This demonstrates that combustion and decomposition of all organic constituent precursors in the samples have been completed below 600 ^oC.

3.1.5 SEM and TEM studies

Morphological aspect of the $CaMoO_4$:Eu nanophosphors of ASP, 600 and 900 ^oC are investigated by taking the SEM and TEM micrographs. Typical SEM morphology of $CaMoO_4$:Eu nanophosphors of ASP, 600 and 900 ^oC heated samples are shown in Fig. 7(a), (b) and (c), respectively. The scale bar indicated on each figure corresponds to size of 100 nm. In ASP, there are agglomerated particles in which one particle contains many small crystallites. Each crystallite has 30-40 nm size. In 600 ^oC, particles are spherical in shape and smallest particle has size of 50-60 nm. In 900 ^oC, bigger aggregates of spherical particles are obtained and smallest particle has size of 350-360 nm. It is observed that as annealing temperature increase, the particle size increases. Particle size distribution histograms for 600 (Fig. 7(b)) and 900 ^oC (Fig. 7(c)) annealed samples are presented in Fig 7(d) and Fig.S5 (ESI), respectively. Mean diameters of the particles for 600 and 900 ^oC annealed $CaMoO_4$:Eu is found to be ~100 and ~500 nm on fitting the histogram with Gaussian function.

Typical TEM micrographs of ASP 5 at.% Gd^{3+} co-doped $CaMoO_4$:Eu are shown in Fig. 8(a). Many crystallites form agglomerated particle. This is similar to SEM observation. HRTEM of 5 at.% Gd^{3+} co-doped $CaMoO_4$:Eu at 900 ^oC is used to calculate *d* spacing and corresponding (*hkl*) plane, which is shown in Fig. 8(c). It confirms that maximum growth of the crystal have been taken along the *(101)* plane and d_{101} = 4.5 Å. To check the growth direction of planes and their corresponding *d* spacing, we have analysed by taking various plane spots in HRTEM, which is shown in Fig. S6 (ESI†) marked as (i), (ii), (iii) and (iv). From this, it is inferred that in most of the cases i.e. at (i), (ii) and (iii) spots, *d* spacing is same as marked in Fig. 8(c). For region marked as (iv), some crystal growth takes place in *(004)* planes with spacing having 2.77 Å which is shown in Fig. S6(c)(ESI†). Energy dispersive spectra (EDS) of ASP 5 at.% Gd^{3+}co-doped $CaMoO_4$:Eu is shown in the Fig. 8(b). EDS analysis reveals the presence of the most intense peaks of Mo along with calcium (Ca), oxygen (O), europium (Eu), gadolinium (Gd) and Cu peaks. Presence of Cu peaks in the EDS spectra are manifestation from the copper micrometer grids. Moreover, no other impurities were pronounced indicating that Gd^{3+}co-doped $CaMoO_4$:Eu phosphors are chemically pure in composition via auto combustion route.

5. Conclusions

Highly crystalline Gd^{3+} (0, 2, 5, 7 and 10 at. %) co-doped $CaMoO_4$:Eu nanoparticles are synthesized under facile auto-combustion route. In order to get the higher crystallinity, ASP sample is heated up to 600 and 900 ^oC. The tetragonal scheelite phase having space group $I4_1/a$ and Z = 4 is found. Extra peaks in XRD patterns are found in case of ASP and 600 ^oC and these are not there in 900 ^oC. FTIR spectrum shows the bands at ~815 cm^{-1} and 427 cm^{-1}, which are due to asymmetric stretching and bending vibrations of O-Mo-O of MoO_4^{2-} tetrahedron, respectively. From XPS study, Ca is found to be +2 oxidation state; while Mo, Eu and Gd are found to be +6, +3 and +3 oxidation states, respectively. Core

binding energy peak at ~141.1 eV corresponds to $Eu^{3+}(4d_{3/2})$. No peak at ~127.1 eV which corresponds to $Eu^{2+}(4d_{5/2})$ is observed. This supports the high probability of Eu^{3+} present in the samples. The particle size increases with annealing.

Acknowledgements

One of the authors (B. P. Singh) is thankful to Ministry of Human Resource and Development (MHRD) for providing senior research teaching assistantship.

References

1 G. S. R. Raju, E. Pavitra, Y. H. Ko and J. S. Yu, *J. Mater. Chem*., 2012, **22,** 15562.

2 A. K. Parchur, R. S. Ningthoujam, S. B. Rai, G. S. Okram, R.A. Singh, M. Tyagi, S.C. Gadkari, R. Tewari and R. K. Vatsa, *Dalton Trans*., 2011,**40,** 7595.

3 E. Cavalli, P. Boutinaud, R. Mahiou, M. Bettinelli and P. Dorenbos, *Inorg. Chem.*, 2010, **49**, 4916.

4 S. Mahlik, M. Behrendt, M. Grinberg, E. Cavalli and M. Bettinelli, *J. Phys.: Condens. Matter*, 2013, **25,** 105502.

5 A. K. Parchur, A. I. Prasad, A. A. Ansari, S. B. Rai and R. S. Ningthoujam, *Dalton Trans.* 2012, **41**, 11032.

6 V. S. Marques, L. S. Cavalcante, J. C. Sczancoski, A. F. P. Alcantara, M. O. Orlandi, E. Moraes, E. Longo, J. A. Varela, M. S. Li and M. R. M. C. Santos, *Crystal Growth & Design*, 2010, **10,** 4752.

7 V. M. Longo, L. S. Cavalcante, E. C. Paris, J. C. Sczancoski, P. S. Pizani, M. S. Li, J. Andres, E. Longo and J. A. Varela, *J. Phys. Chem. C,* 2011, **115,** 5207.

8 A. K. Parchur and R. S. Ningthoujam, *Dalton Trans*., 2011, **40,** 7590.

9 S. Acharya, U. K. Gautam, T. Sasaki, Y. Bando, Y. Golan and K. Ariga, *J. Am. Chem. Soc*., 2008, **130**, 4594.

10 K. Ariga, A. Vinu, Y. Yamauchi, Q. Ji and J. P. Hill, *Bull. Chem. Soc. Jpn*., 2012, **85**, 1.

11 A. Vinu and K. Ariga, *Advanced Porous Materials*, 2013, **1**, 63.

12 A. Kar and A. Patra, *Nanoscale*, 2012, **4**, 3608.

13 B. K. Gupta, V. Rathee, T. N. Narayanan, P. Thanikaivelan, A. Saha, Govind, S. P. Singh, A. A. Marti and P. M. Ajayan, *Small*, 2011, **7**, 1767.

14 H. Guo, Z. Li, H. Qian, Y. Hu and I. N. Muhammad, *Nanotechnology*, 2010, **21**, 125602.

15 N. O. Nunez, S. Rivera, D. Alcantara, J. M. Fuente, J. G. Sevillano and M. Ocana, *Dalton Trans*., 2013, **42**, 10725.

16 A. Podhorodecki, M. Bański, J. Misiewicz, J. Serafińczuk, and N. V. Gaponenko, *J. Electrochem. Soc*., 2010, **157**, H628.

17 A. Podhorodecki, G. Zatryb, J. Misiewicz, D. Kaczmarek, J. Domaradzki and A. Borkowska, *J. Electrochem. Soc.*, 2009, **156**, H214.

18 A. Podhorodecki, J. Misiewicz, F. Gourbilleau and C. Dufour, *Electrochem. Solid-State Lett*., 2010, **13**, K26.

19 A. Podhorodecki, R. Kudrawiec, M. Nyk, J. Misiewicz, and W. Strek, *Opt. Mater*., 2009, **31**, 1252.

20 S. Yu, Z. Lin, L. Zhang and G. Wang, *Crystal Growth & Design*, 2007, **7**, 7595.

21 Z. Qiu, Y. Zhou, M. Lu, J. Zhou, A. Zhang, Z. Yang and Q. Ma, *Nanotechnology*, 2007, **17**, 495705.

22 J. Rodriguez- Carvajal, FULLPROF a Rietveld and pattern matching analysis program, Laboratoire Leon Brillouin (CEA-CRNS), Paris France.

23 R. D. Shanon, *Acta Crystallogr*., *Sect. A: Cryst. Phys., Diffr*., *Theor. Gen. Crystallogr*., 1976, **32**, 751.

24 A. Kar, A. Dutta and A. Patra, *J. Mater. Chem*., 2010, **20**, 916.

25 S. Dutta, S. Som and S. Sharma, *Dalton Trans*., 2013, **42**, 9654.

26 S. Yan, J. Zhang, X. Zhang, S. Lu, X. Ren, Z. Nie and X. Wang, *J. Phys. Chem. C*, 2007, **111**, 13256.

27 D. L. Rousseau, R. P. Bauman and S. P. S. Porto, *J. Raman Spectrosc*. 1981, **10**, 253.

28 S. P. S. Porto and J. F. Scott, *Phys. Rev.* 1967, **157**, 716.

29 A. Golubovic, R. Gajic, Z. D. Mitrovic and S. Nikolick, *J. Alloys. Comp*., 2006, **415**, 16.

30 M. N. Luwang, R. S. Ningthoujam, Jagannath, S. K. Srivastava and R. K. Vatsa, *J. Am. Chem. Soc*., 2010, **132**, 2759.

31 F. Lei and B. Yan, *J. Solid State Chem*., 2008, **181**, 855.

32 P. Yang, C. Li, W. Wang, Z. Quan, S. Gai and J. Lin, *J. Solid State Chem*., 2009, **182**, 2510.

33 S. I. Woo, J.S. Kim and H. K. Jun, *J. Phys. Chem. B*, 2004, **108**, 8941.

34 G. D. Khattak, M. A. Salim, A. S. Al. Harthi, D. J. Thompson and L. E. Wenger, *J. Non-Cryst. Solids*, 1997, **212**, 180.

35 L. Zhou, Z. Gu, X. Liu, W. Yin, G. Tian, L. Yan, S. Jin, W. Ren, G. Xing, W. Li, X. Chang, Z. Hu and Y. Zhao, *J. Mater. Chem*., 2012, **22**, 966.

36 L. R. Shah, B. Ali, H. Zhu, W. G. Wang, Y. Q. Song, H. W. Zhang, S. I. Shah and J. Q. Xiao, *J. Phys.: Condens. Matter*, 2009, **21**, 486004.

37 A. K. Parchur, A. I. Prasad, S. B. Rai, R. Tewari, R. K. Sahu, G. S. Okram, R. A. Singh and R. S. Ningthoujam, *AIP Advances*, 2012, **2**, 032119.

Table 1 Calculated values of *a*, *c*, *V* and *D* for Gd^{3+} (0, 2, 5, 7 and 10 at %) co-doped $CaMoO_4$:Eu at 600 ^oC and 900 ^oC.

	600 ^oC				900 ^oC			
Gd^{3+}	*a*	*c*	*V*	*D*	*a*	*c*	*V*	*D*
0	5.224(2)	11.446(5)	312.11(19)	38	5.224(2)	11.439(4)	312.14(18)	59
2	5.223(2)	11.437(5)	311.97(02)	48	5.225(2)	11.434(3)	312.15(16)	61
5	5.226(2)	11.440(5)	312.28(02)	52	5.227(2)	11.437(5)	312.37(22)	62
7	5.226(2)	11.433(5)	312.25(19)	54	5.227(2)	11.431(4)	312.31(17)	71
10	5.226(2)	11.442(5)	312.16(21)	57	5.227(2)	11.429(5)	312.27(19)	69

Graphical abstract

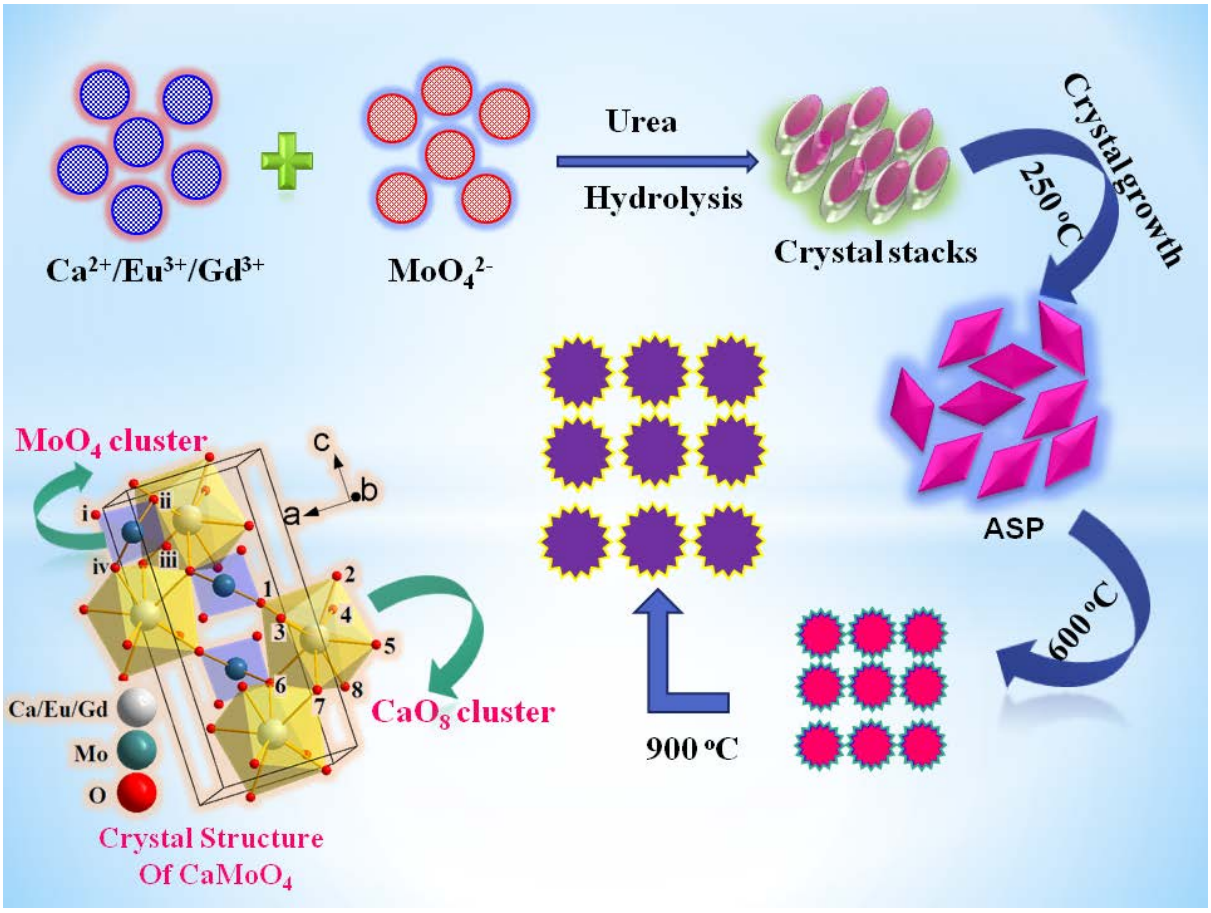

Represents the growth mechanism involved in the facile auto-combustion route and simplified polyhedral representation showing [CaO_8] and [MoO_4] clusters of Gd^{3+} co-doped $CaMoO_4$:Eu nanoparticles.

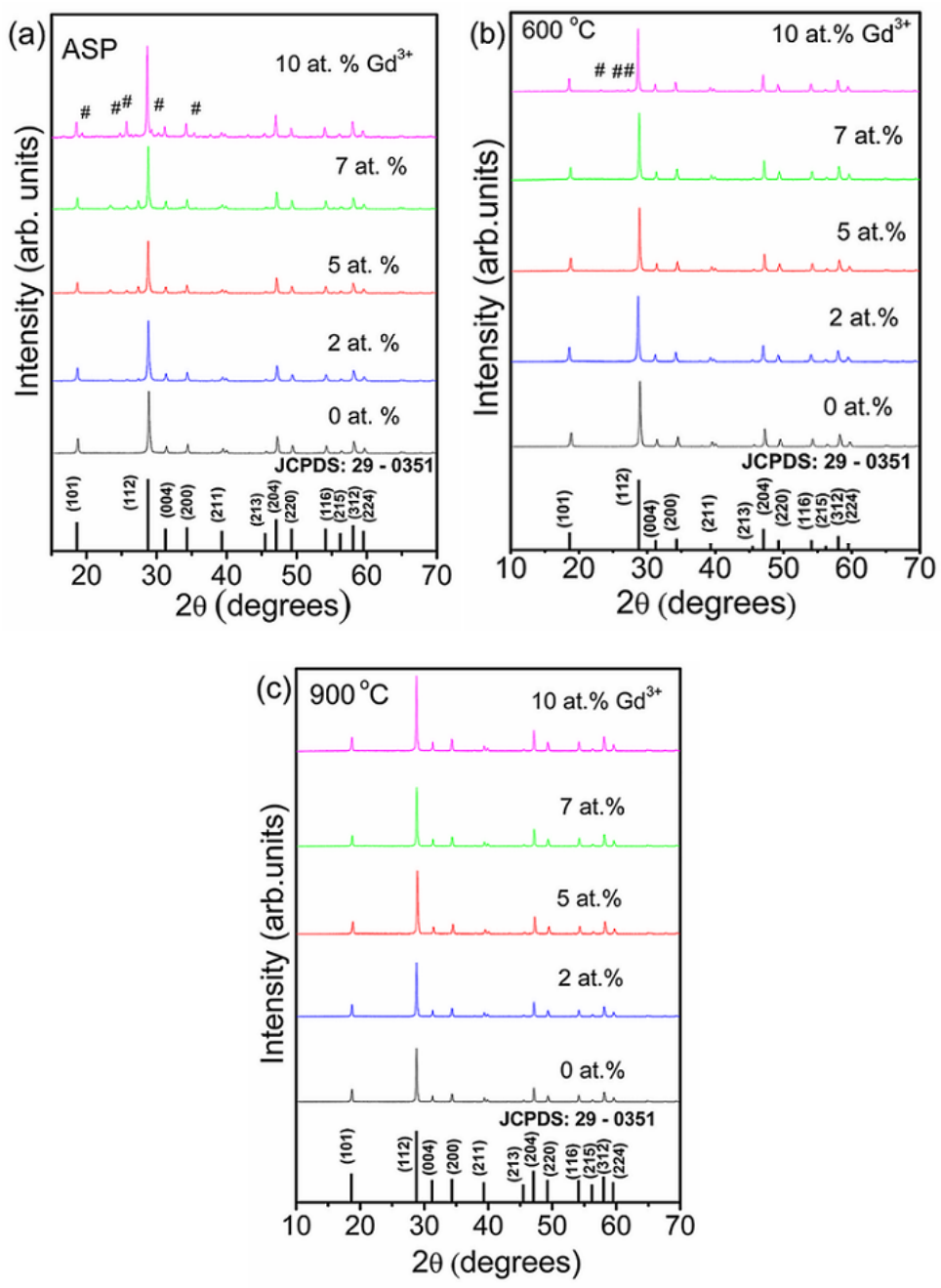

Fig. 1 (a), (b) and (c) XRD patterns of Gd^{3+}(0, 2, 5, 7 and 10 at.%) co-doped $CaMoO_4$:Eu for ASP, 600 and 900 ^oC samples, respectively. Atomic percentage of Gd^{3+} is given in figure itself. The symbol # represents the extra phase evolution.

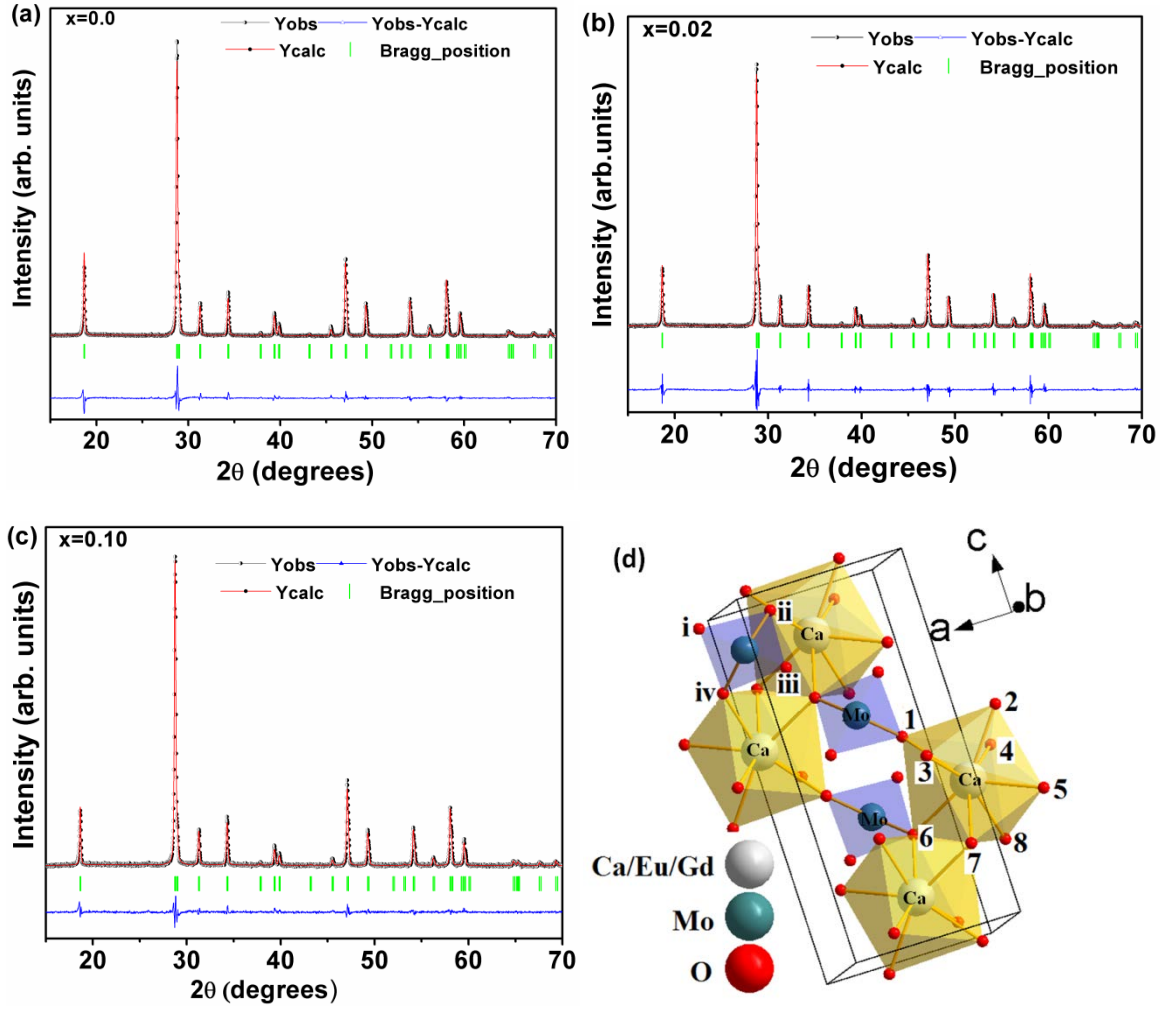

Fig.2 (a), (b), (c) Rietveld plot of 0, 2 and 10 at.% Gd^{3+} co-doped $CaMoO_4$:Eu samples annealed at 900 ^oC and (d) simplified polyhedral representation of Gd^{3+} co-doped $CaMoO_4$:Eu having both [CaO_8] and [MoO_4] clusters.

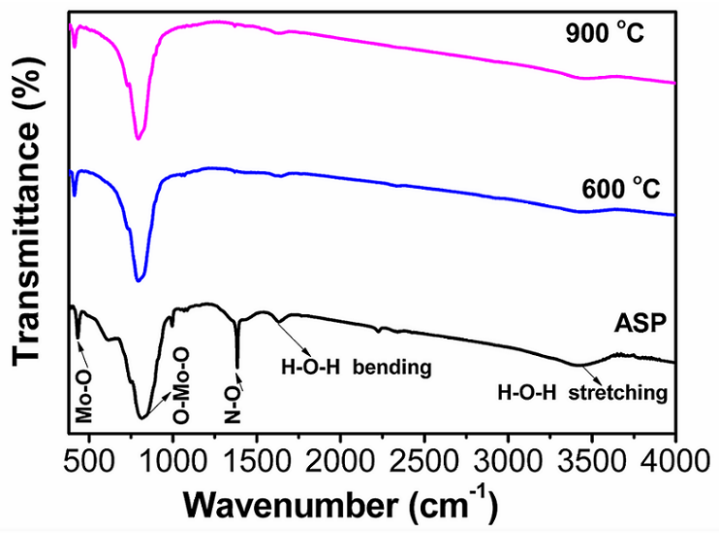

Fig.3 FTIR spectra of ASP, 600 and 900 °C annealed samples of 5 at.% Gd^{3+} co-doped $CaMoO_4$:Eu .

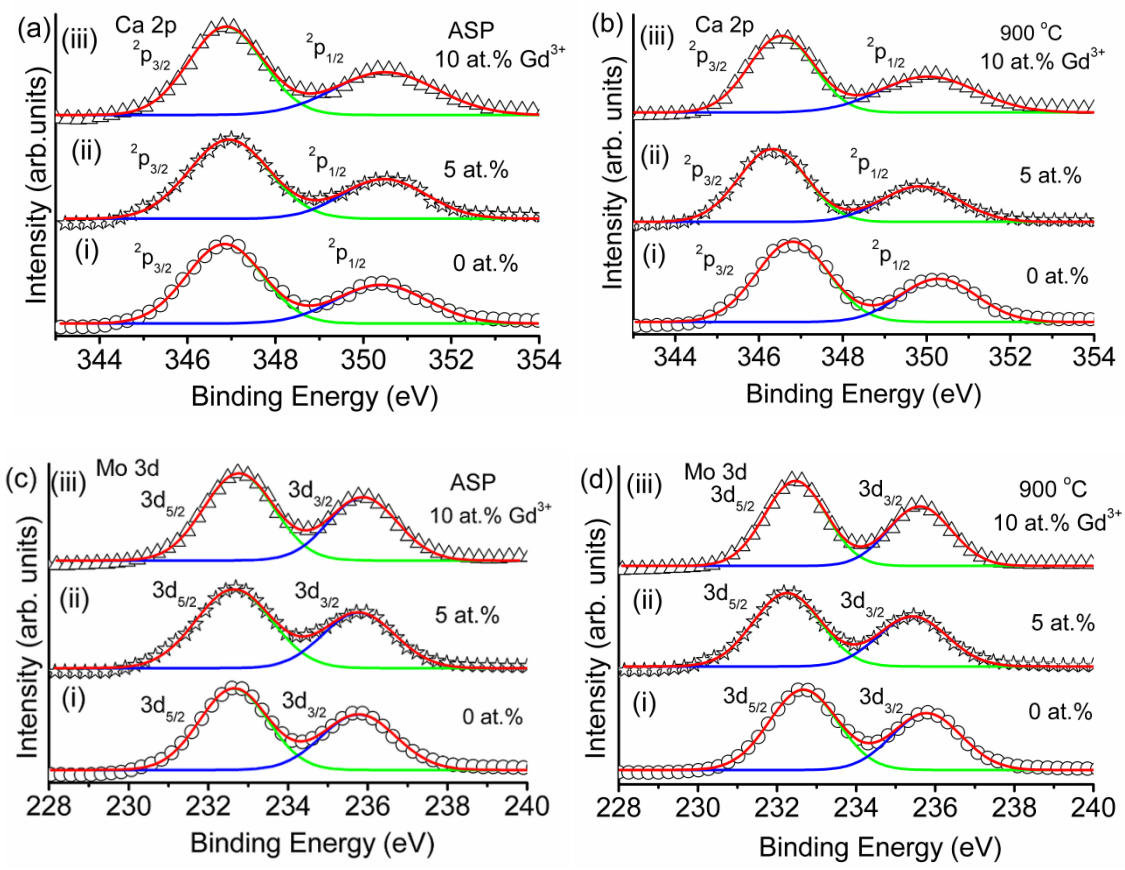

Fig.4 XPS spectra of as-prepared and 900 ^oC annealed samples 0, 5 and 10 at.% Gd^{3+} co-doped $CaMoO_4$:Eu. Peaks corresponding to the core binding energies of individual elements viz, Ca and Mo are shown in Fig. (a)-(d).

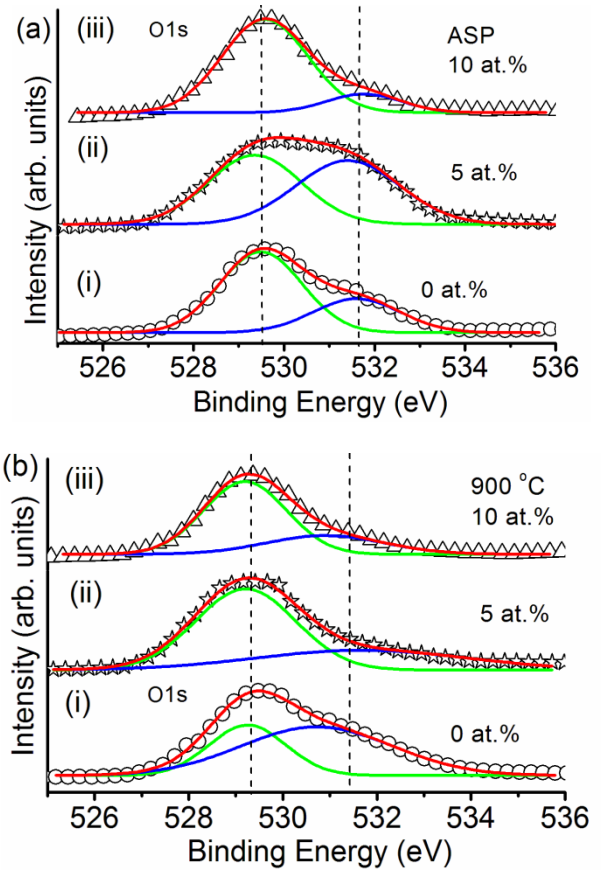

Fig.5 XPS spectra of O1s for (a) ASP and (b) 900 ^{o}C annealed, Gd^{3+} (0, 5 and 10 at.%) co-doped $CaMoO_4$:Eu.

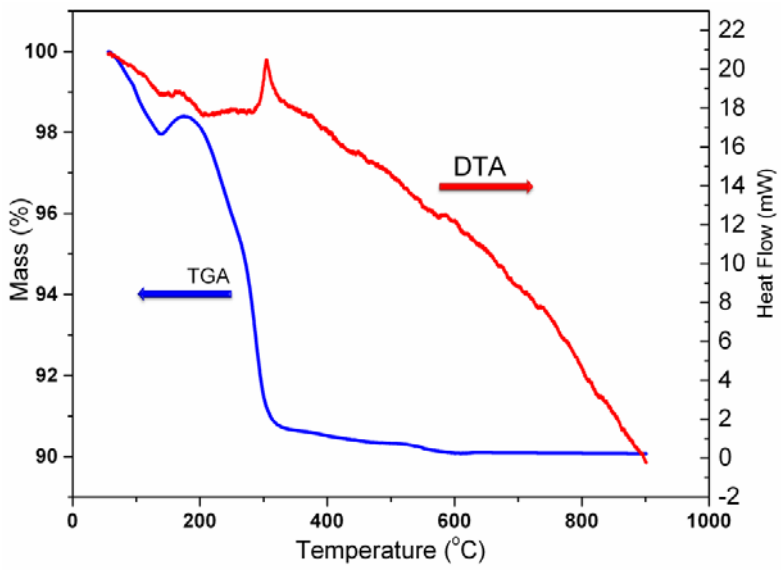

Fig. 6 TG-DTA curves of as-prepared precursor for $CaMoO_4$:Eu in synthetic air.

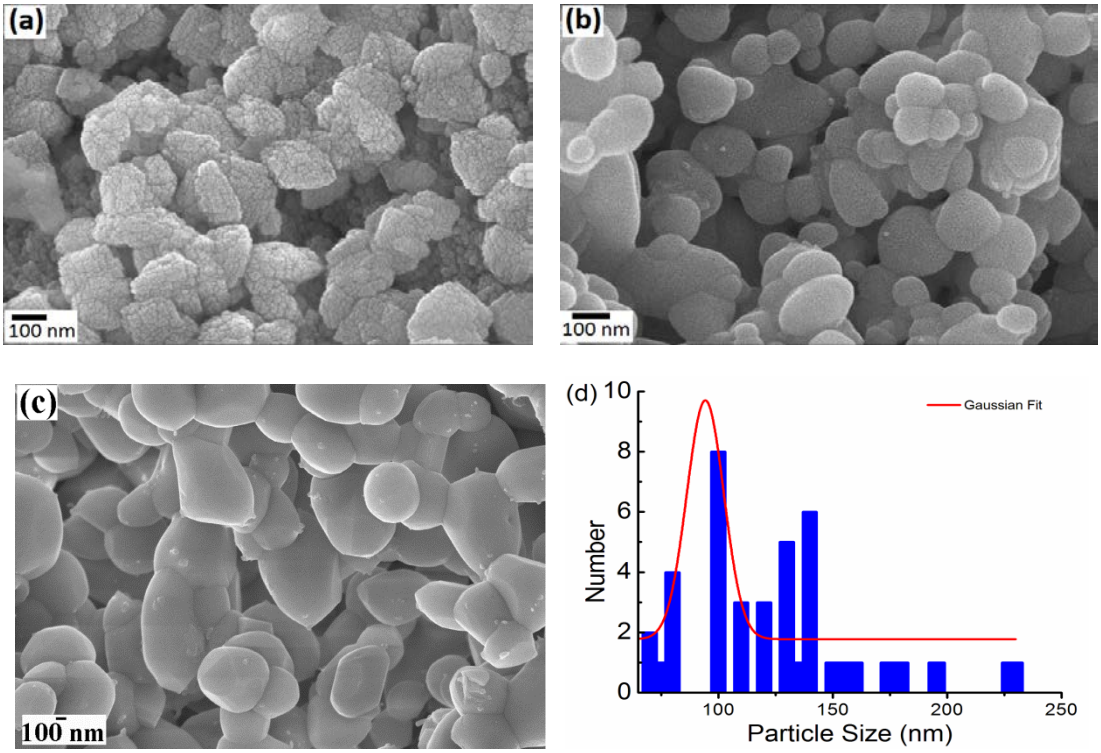

Fig. 7 FE-SEM images of micro-spherical particles $CaMoO_4$:Eu for (a) as-prepared (b) 600 (c) annealed at 900 ^oC and (d) particle size distribution for 600 ^oC annealed samples.

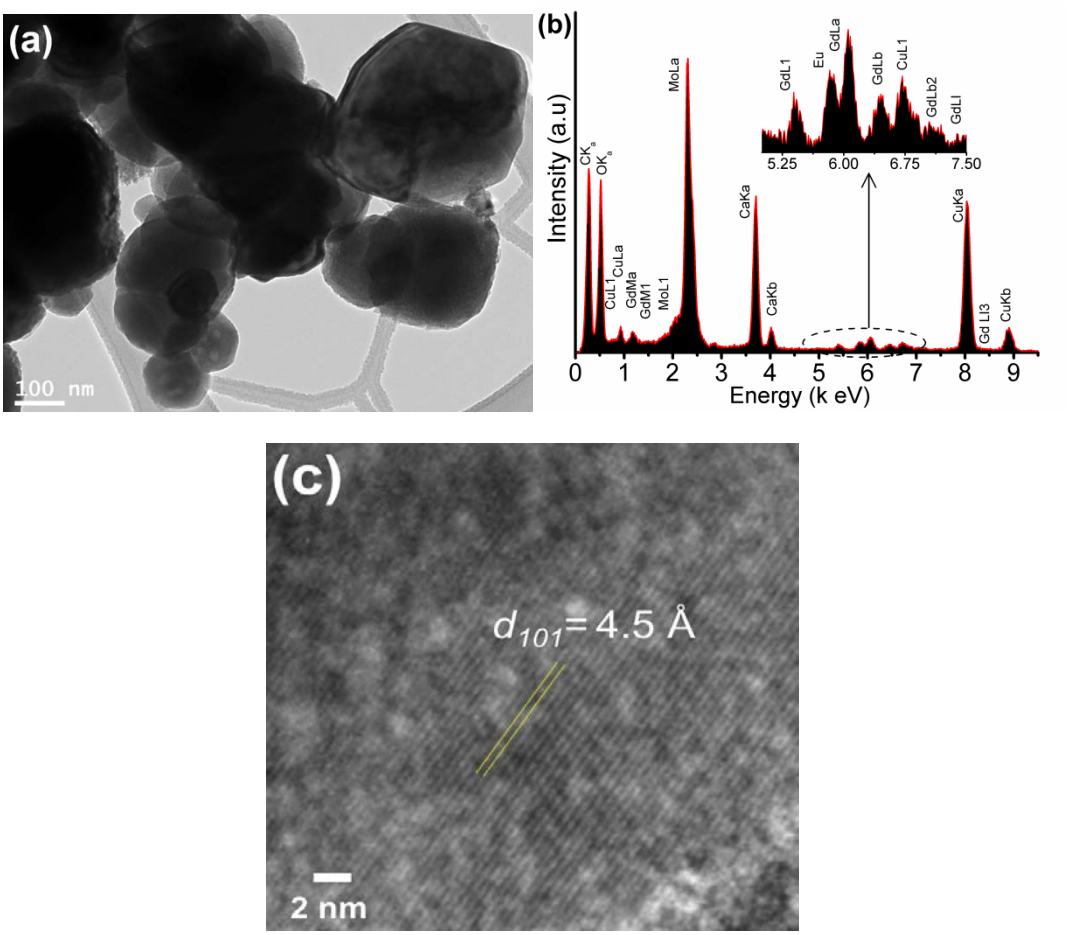

Fig. 8(a) TEM and (b) shows the elemental composition of a large area of ASP 5at.% Gd^{3+} co-doped $CaMoO_4$:Eu nanophosphors, which is verified by the presence of Ca, Mo, Eu and Gd peaks. Cu peak comes from the Copper grid used for the electron microscopy analysis and (c) HRTEM images of 5 at.% Gd^{3+} co-doped $CaMoO_4$:Eu at 900 ^oC.